ANTIOXIDANTS & REDOX SIGNALING
Volume 17, Number 12, 2012

DOI: 10.1089/ars.2011.4294

ORIGINAL RESEARCH COMMUNICATION

Trolox-Sensitive Reactive Oxygen Species Regulate Mitochondrial Morphology, Oxidative Phosphorylation and Cytosolic Calcium Handling in Healthy Cells

Felix Distelmaier,[1–3,*] Federica Valsecchi,[1,2,*,†] Marleen Forkink,[1] Sjenet van Emst-de Vries,[1] Herman G. Swarts,[1] Richard J.T. Rodenburg,[2] Eugène T.P. Verwiel,[4] Jan A.M. Smeitink,[2] Peter H.G.M. Willems,[1] and Werner J.H. Koopman[1]

Abstract

Aims: Cell regulation by signaling reactive oxygen species (sROS) is often incorrectly studied through extracellular oxidant addition. Here, we used the membrane-permeable antioxidant Trolox to examine the role of sROS in mitochondrial morphology, oxidative phosphorylation (OXPHOS), and cytosolic calcium (Ca^{2+}) handling in healthy human skin fibroblasts. ***Results and Innovation:*** Trolox treatment reduced the levels of 5-(and-6)-chloromethyl-2′,7′-dichlorodihydro-fluorescein (CM-H_2DCF) oxidizing ROS, lowered cellular lipid peroxidation, and induced a less oxidized mitochondrial thiol redox state. This was paralleled by increased glutathione- and mitofusin-dependent mitochondrial filamentation, increased expression of fully assembled mitochondrial complex I, elevated activity of citrate synthase and OXPHOS enzymes, and a higher cellular O_2 consumption. In contrast, Trolox did not alter hydroethidium oxidation, cytosolic thiol redox state, mitochondrial NAD(P)H levels, or mitochondrial membrane potential. Whole genome expression profiling revealed that Trolox did not trigger significant changes in gene expression, suggesting that Trolox acts downstream of this process. Cytosolic Ca^{2+} transients, induced by the hormone bradykinin, were of a higher amplitude and decayed faster in Trolox-treated cells. These effects were dose-dependently antagonized by hydrogen peroxide. ***Conclusions:*** Our findings suggest that Trolox-sensitive sROS are upstream regulators of mitochondrial mitofusin levels, morphology, and function in healthy human skin fibroblasts. This information not only facilitates the interpretation of antioxidant effects in cell models (of oxidative-stress), but also contributes to a better understanding of ROS-related human pathologies, including mitochondrial disorders. *Antioxid. Redox Signal.* 17, 1657–1669.

Introduction

WITHIN THE LIVING CELL, mitochondrial structure displays a large variability ranging from spherical to filamentous (1). Net mitochondrial morphology depends on the balance between mitochondrial fusion and fission (47), which are mediated by the action of dynamin-related GTPases, including two mitofusin isoforms (mitofusin 1 [Mfn1], mitofusin 2 [Mfn2]; fusion), dynamin-related protein 1 (Drp1; fission), and human fission protein 1 (hFis1; fission). It appears that mitochondrial morphology is cell-type specific and linked to the respiratory activity of the mitochondrial electron transport chain (ETC) (47). The latter sustains the inward-directed proton motive force (PMF) across the mitochondrial inner membrane (MIM) and consists of a chemical (ΔpH) and electrical component (mitochondrial membrane potential

[1]Department of Biochemistry, Nijmegen Centre for Molecular Life Sciences, Radboud University Nijmegen Medical Centre, Nijmegen, The Netherlands.
[2]Department of Pediatrics, Nijmegen Centre of Mitochondrial Disorders, Radboud University Nijmegen Medical Centre, Nijmegen, The Netherlands.
[3]Department of General Pediatrics and Neonatology, University Children's Hospital, Heinrich-Heine-University, Düsseldorf, Germany.
[4]Department of Human Genetics, Radboud University Nijmegen Medical Centre, Nijmegen, The Netherlands.
*These authors are joint first authors.
†*Current affiliation:* Department of Neurology and Neuroscience, Weill Cornell Medical College, New York, New York.

Innovation

Our results support a model (Fig. 7) in which 5-(and-6)-chloromethyl-2′,7′-dichlorodihydro-fluorescein (CM-H_2DCF) oxidizing signaling reactive oxygen species (sROS; and/or their downstream products) control mitochondrial morphology in a glutathione- and mitofusin-dependent manner. Trolox lowers these sROS levels, thereby stimulating mitochondrial filamentation, oxidative phosphorylation activity, and routine/maximal O_2 consumption. In parallel, Trolox treatment reduces the inhibition of sarcoplasmatic-endoplasmatic reticulum Ca^{2+} ATPase (SERCAs) by CM-H_2DCF-oxidizing sROS, possibly *via* lowering endoplasmic reticulum (ER) lipid peroxidation. Alternatively, improved mitochondria-ER tethering might facilitate the local supply of mitochondrial ATP to the SERCA pumps. As a consequence, Trolox treatment increases ER Ca^{2+} content and the amplitude and decay rate of hormone-induced cytosolic Ca^{2+} transients, which constitute an important second-messenger signaling system.

[$\Delta\psi$]). A proper PMF is required for mitochondrial ATP generation by the F_oF_1-ATPase and a variety of other energy-dependent processes such as metabolite/ion exchange with the cytosol and the import of mitochondrial proteins encoded by the nuclear DNA (27). Mitochondrial fragmentation is often observed during pathological conditions and is associated with low cellular energy demand and ETC activity (47). In contrast, high ETC activity was linked to the establishment of a mitochondrial reticulum or "hyperfused network" (47). Evidence was provided that the fragmented state allows mitophagy of individual organelles that are damaged and/or energetically compromised (*e.g.*, Refs. 39, 40), whereas filamentous mitochondria are spared from degradation during autophagy, allowing the maintenance of ATP production and cell survival (13). It was further proposed that a highly interconnected mitochondrial network protects from stochastic depletion of metabolic substrates or mitochondrial DNA and facilitates the sharing/transport of intra-mitochondrial constituents such as metabolites, macromolecules, and antioxidants (31). Antioxidant sharing appears to prevent oxidative stress in filamentous mitochondria by making them less susceptible to reactive oxygen species (ROS) (29).

ROS can be formed on the partial reduction of molecular oxygen (O_2) in various cell compartments (2) and include the superoxide anion ($O_2^{\bullet -}$) and hydrogen peroxide (H_2O_2). Depending on the concentration and lifetime of the particular ROS involved, they can act as signaling molecules "sROS" or induce oxidative stress when their levels exceed the capacity of cellular antioxidant systems (3, 10, 22, 30, 48). Often, the signaling and damaging pathways are intertwined when increased ROS production triggers adaptive up-regulation of ROS detoxifying homeostatic systems (*e.g.*, 27, 37). The analysis of primary human fibroblasts from patients with an isolated deficiency in the first ETC complex (CI) revealed that greatly increased cellular ROS levels were associated with a fragmented mitochondrial morphology (25). We proposed that mitochondrial fragmentation occurs as a consequence of very high ROS levels, which is compatible with other studies revealing that the extracellular application of H_2O_2 and light-induced oxidative stress induce mitochondrial fragmentation (8, 18, 32, 49). Mechanistic evidence was presented which stated that H_2O_2 stimulates ubiquitin-mediated breakdown of Mfn1/2 but not of hFis1 in primary human skin fibroblasts (33). If this is a general mechanism, then sROS levels in healthy cells might also be involved in the regulation of mitochondrial morphology, and the lowering of these ROS levels should stimulate mitochondrial filamentation. On the other hand, during hyperglycemic conditions, mitochondrial fragmentation was strictly required for enhanced mitochondrial ROS production (50, 51), supporting a mechanism where increased ROS production is a downstream consequence of mitochondrial fragmentation.

Currently, it is unclear whether and how sROS play a role in the regulation of mitochondrial morphology and function in healthy cells. To address this question, one could increase ROS levels throughout the cell by adding an extracellular oxidant and studying the consequences of this maneuver on mitochondrial and cellular physiology. However, the downstream cellular responses to ROS are a function of its subcellular origin (28). Moreover, it is difficult to control the intracellular ROS concentration by adding ROS exogenously. The latter is important, as the chronic application of exogenous ROS (*e.g.*, H_2O_2) induces concentration-dependent effects ranging from growth stimulation (3–15 μM) to temporary growth arrest (120–150 μM), permanent growth arrest (250–400 μM), and necrotic cell death ($\geq$1 mM) (15). Another aspect is that the cytotoxicity of H_2O_2 in cell cultures can vary widely with incubation time and cell concentration, because cells remove H_2O_2 from the culture medium (15). To investigate our hypothesis that lowering sROS levels in healthy cells should stimulate mitochondrial filamentation and avoid potential problems associated with the use of exogenous oxidants, we applied a "reverse" strategy here. The latter consisted of studying the consequences of sROS level reduction by exogenous application of the vitamin E analog Trolox (6-hydroxy-2,5,7,8-tetramethylchroman-2-carboxylic acid), a widely used phenolic antioxidant (4, 38). Our results support a model in which Trolox-sensitive sROS regulate mitochondrial mitofusin levels and thereby mitochondrial morphology and function in healthy cells.

Results

Trolox reduces 5-(and-6)-chloromethyl-2′,7′-dichlorodihydro-fluorescein oxidation and cellular lipid peroxidation but not hydroethidium oxidation

Trolox treatment of primary human skin fibroblasts did not affect the oxidation rate of the ROS-sensor hydroethidium (HEt) but lowered this parameter for the ROS-sensor 5-(and-6)-chloromethyl-2′,7′-dichlorodihydro-fluorescein (CM-H_2DCF; Fig 1A). This effect was paralleled by a lowering of cellular lipid peroxidation (Fig. 1B) and a reduction in the extent of oxidation of the thiol redox environment in the mitochondrial matrix but not in the cytosol (Fig. 1C). Trolox did not alter mitochondrial NAD(P)H levels (Fig. 1D).

Trolox stimulates mitochondrial filamentation

A computer-assisted analysis of mitochondrial morphology revealed that Trolox increased the mitochondrial

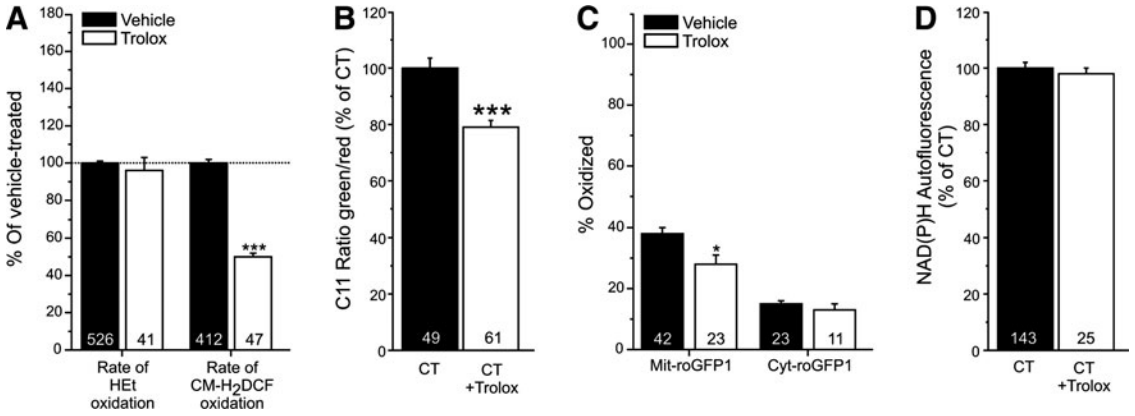

FIG. 1. Hydroethidium (HEt) and 5-(and-6)-chloromethyl-2′,7′-dichlorodihydro-fluorescein (CM-H_2DCF) oxidation, lipid peroxidation, thiol redox status, and mitochondrial NAD(P)H levels in human skin fibroblasts treated with Trolox. (A) Effect of Trolox on the rate of HEt and CM-H_2DCF oxidation. **(B)** Effect of Trolox on cellular lipid peroxidation as reflected by the fluorescence emission ratio between the green (oxidized) and red (reduced) forms of C11-BODIPY$^{581/591}$ (C11). **(C)** Effect of Trolox on the thiol redox status in the mitochondrial matrix (Mit) and cytosol (Cyt), as reported by a redox-sensitive fluorescent protein (roGFP1). **(D)** Effect of Trolox on mitochondrial NAD(P)H autofluorescence. In this figure, significant differences with vehicle (CT) are marked by *($p < 0.05$) and ***($p < 0.001$). Numerals (N) reflect the number of cells analyzed in at least two independent experiments.

formfactor (F), which is a combined measure of mitochondrial length and degree of branching, without altering the number of mitochondria per cell (Nc; Fig. 2A, B). Culturing the cells in the presence of 10 nM (24) of the MIM-targeted antioxidant mitoquinone (MitoQ) for 96 h did not significantly affect mitochondrial morphology (Fig. 2A, B).

Trolox-induced mitochondrial filamentation requires glutathione

The tripeptide glutathione (GSH) is an important determinant of the thiol redox environment and is involved in the recycling of Trolox radicals (34). We previously demonstrated that the inhibition of GSH synthesis by L-buthionine-(S,R)-sulphoximine (BSO; 12.5 μM, 72 h) shifts the cytosolic and mitochondrial thiol redox environment toward a fully oxidized state in human skin fibroblasts (43). Here, BSO not only fully prevented the Trolox-induced increase in F but even decreased this parameter (Fig. 2A, B). Moreover, Nc increased in cells treated with Trolox + BSO. These results suggest that a shift in the cytosolic and mitochondrial thiol redox environment toward a more oxidized state stimulates mitochondrial shortening and that Trolox-induced stimulation of mitochondrial filamentation requires GSH.

Trolox increases mitochondrial Mfn2 protein levels

Changes in mitochondrial morphology are mediated by the action of dynamin-related GTPases, including mitofusins, Drp1, and hFis1. Western blot analysis of mitochondria-enriched fractions revealed that Trolox increased the mitochondrial level of Mfn2 in primary human skin fibroblasts without affecting these levels for Drp1 and hFis1 (Fig. 3A, B). Trolox similarly affected mitochondrial morphology (Fig. 3C, D) and Mfn2 expression (Fig. 3E, F) in Chinese Hamster Ovary (CHO) cells. These results suggest that the Trolox-induced increase in mitochondrial filamentation is mediated by Mfn2 and is not an exclusive feature of primary human skin fibroblasts.

Trolox-induced mitochondrial filamentation requires mitofusins

To dissect the role of the two mitofusin isoforms (Mfn1 and Mfn2) in Trolox-induced mitochondrial filamentation, we determined the effect of Trolox treatment on mitochondrial morphology (Fig. 4A, B) in immortalized wild-type (wt) mouse embryonic fibroblasts (MEFs) and cells lacking both Mfn1 and Mfn2 (mitofusin 1 and 2 double knockout [$Mfn1^{-/-}Mfn2^{-/-}$]), Mfn1 ($Mfn1^{-/-}$), or Mfn2 ($Mfn2^{-/-}$). In wt MEFs, Trolox treatment greatly increased F (Fig. 4C) and reduced Nc (Fig. 4D), which is compatible with increased mitochondrial filamentation and fusion. Trolox did not affect $\Delta\psi$ in wt MEFs (Fig. 4E). $Mfn1^{-/-}Mfn2^{-/-}$ MEFs displayed a reduced F and Nc as well as $\Delta\psi$ hyperpolarization, all of which were not substantially affected by Trolox (Fig. 4C–E). $Mfn1^{-/-}$ MEFs displayed a reduced F and an increased Nc, indicative of massive mitochondrial fragmentation, which was not normalized by Trolox. In contrast, $\Delta\psi$ hyperpolarization in $Mfn1^{-/-}$ cells was restored to wt level by Trolox treatment. In case of $Mfn2^{-/-}$ MEFs, F was reduced relative to wt cells, albeit to a lesser extent than for $Mfn1^{-/-}Mfn2^{-/-}$ and $Mfn1^{-/-}$ cells (Fig. 4C); whereas Nc was not affected (Fig. 4D). On Trolox treatment, the reduced F and $\Delta\psi$ hyperpolarization were fully normalized to wt level in $Mfn2^{-/-}$ MEFS, whereas Nc was not affected. Taken together, the data presented in Figures 3 and 4 demonstrate that the Trolox-induced stimulation of mitochondrial filamentation requires the presence of mitofusins.

Mitochondrial fragmentation is not by default associated with increased ROS levels

The fact that Trolox reduces the levels of CM-H_2DCF oxidizing ROS and stimulates mitochondrial filamentation in a mitofusin-dependent manner suggests that Trolox-sensitive

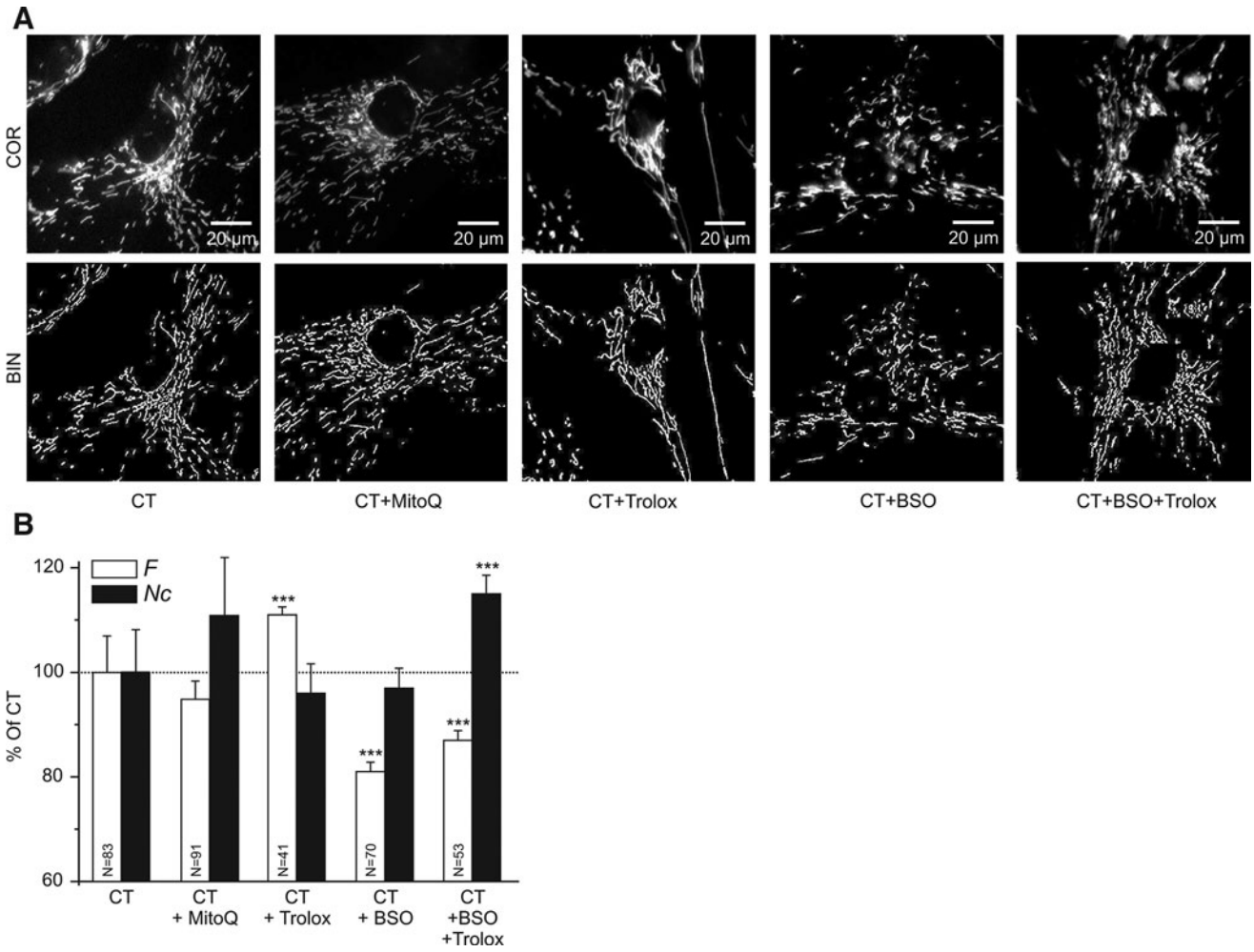

FIG. 2. Effect of anti- and pro-oxidants on mitochondrial structure in human skin fibroblasts. (A) Typical examples of background-corrected confocal images (COR; *upper row*) and their binarized equivalents (BIN; *lower row*) highlighting mitochondrial structure (*white objects*) in human skin fibroblasts stained with rhodamine 123. Cells were cultured in the presence of vehicle (CT), the mitochondrial inner membrane-targeted antioxidant MitoQ (CT + MitoQ), the antioxidant Trolox (CT + Trolox), the GSH-synthesis inhibitor L-buthionine-(S,R)-sulphoximine (BSO) (CT + BSO), or BSO and Trolox together (CT + BSO + Trolox). **(B)** Quantification of the effect of the different treatments on mitochondrial length and degree of branching (reflected by the formfactor *F*), and the number of mitochondria per cell (represented by *Nc*). In this figure, significant differences with CT are marked by ***($p < 0.001$). Numerals (*N*) reflect the number of cells analyzed in at least two independent experiments.

sROS are upstream regulators of mitochondrial morphology. However, Trolox might also directly stimulate mitochondrial filamentation, thereby reducing CM-H_2DCF oxidizing ROS levels. This suggests that mitochondrial fragmentation should increase these levels. To investigate this hypothesis, we determined whether forced mitochondrial fragmentation affected the level of CM-H_2DCF oxidizing ROS in an inducible Drp1-expressing HeLa cell line. Drp1 induction increased cellular Drp1 amounts by 60% (Supplementary Fig. S1A, B; Supplementary Data are available online at www.liebertpub.com/ars), accompanied by a decrease in *F* and an increase in *Nc*, which are indicative of mitochondrial fragmentation (Supplementary Fig. S1C, D). However, the levels of CM-H_2DCF oxidizing ROS did not differ between non-induced and induced cells (Supplementary Fig. S1E), demonstrating that mitochondrial fragmentation not necessarily leads to increased levels of these ROS. Combined with our data presented thus far, these findings support a model in which CM-H_2DCF oxidizing sROS can act as upstream regulators of mitochondrial morphology.

Trolox stimulates routine and maximal O_2 consumption in intact cells

We next determined whether Trolox affected mitochondrial respiratory chain function *in situ* by assessing O_2 consumption in intact fibroblasts using high-resolution respirometry (Fig. 5A). In Trolox-treated cells, routine (R) and maximal O_2-consumption (E) was significantly increased, whereas leak (L) and minimal O_2-consumption (ROX) was not affected. Subsequent addition of the specific CIII inhibitor antimycin A (2.5 μM) did not further reduce ROX (not shown).

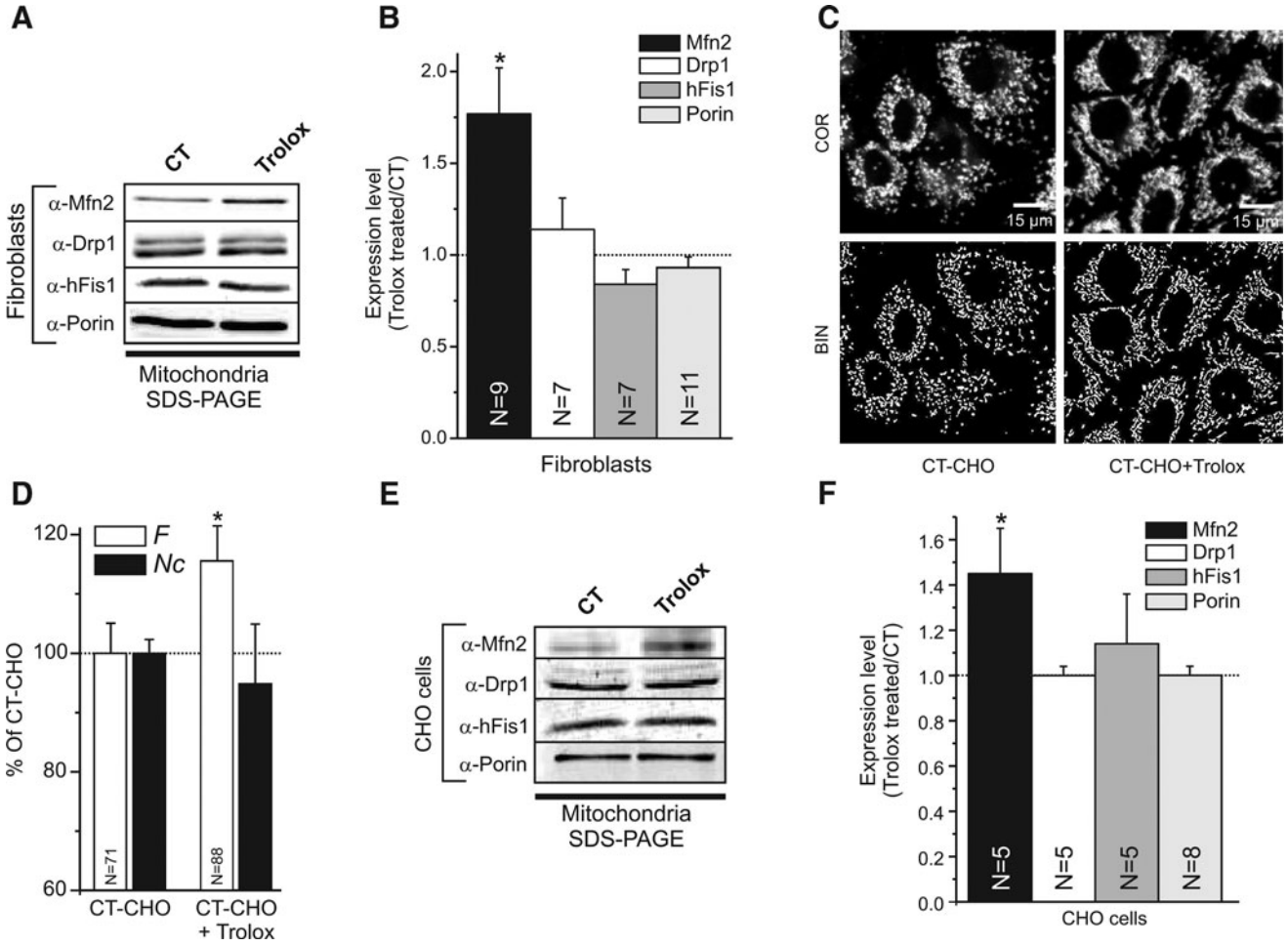

FIG. 3. Effect of Trolox on the expression of mitochondrial fusion and fission proteins in human skin fibroblasts and Chinese Hamster Ovary (CHO) cells. (A) Typical Western blots of mitochondria-enriched fractions showing the expression of the mitochondrial fusion protein Mfn2 (α-Mfn2), the fission proteins Drp1 (α-Drp1) and hFis1 (α-hFis1), and mitochondrial porin (α-porin) in vehicle- (CT) and Trolox-treated human skin fibroblasts. The two bands for Drp1 represent the brain (*upper band*) and ubiquitous (*lower band*) isoform. **(B)** Quantitative analysis of Mfn2, Drp1, hFis1, and Porin levels in Trolox-treated human skin fibroblasts. Expression levels are represented by the ratio between the Trolox-treated and CT condition. **(C)** Typical examples of background-corrected confocal images (COR; *upper row*) and their binarized equivalents (BIN; *lower row*) highlighting the mitochondrial structure (*white objects*) in CHO cells stained with rhodamine 123. CT-CHO and CT-CHO + Trolox indicate vehicle-treated and Trolox-treated cells, respectively **(D)** Quantification of the effect of Trolox treatment on mitochondrial length and degree of branching (reflected by the formfactor *F*), and the number of mitochondria per cell (represented by *Nc*) in CHO cells. **(E)** Same as panel **A**, but now for CHO cells. **(F)** Same as panel **B,** but now for CHO cells. In this figure, significant differences between the CT- and Trolox-treated condition are marked by *($p < 0.05$). Numerals (*N*) reflect the number of independent blots **(B** and **F)** or the number of individual cells **(D)** analyzed in at least two different experiments.

Compatible with the results in wt MEFs (Fig. 4E), Trolox treatment did not affect $\Delta\psi$ in primary human skin fibroblasts (7) (Fig. 5B).

Trolox differentially increases the protein levels of fully assembled oxidative phosphorylation complexes

Increased routine and maximal O_2-consumption are compatible with our previous result that Trolox increases the amount and in-gel activity of fully assembled mitochondrial CI in healthy human skin fibroblasts (23). Using native gel electrophoresis, we observed here that Trolox treatment does not alter the levels of fully assembled CII and CIII, whereas it slightly increases these levels for CIV and CV (Fig. 5C).

Trolox stimulates the maximal activity of citrate synthase and mitochondrial oxidative phosphorylation enzymes

To establish whether Trolox affected the maximal activity (V_{max}) of key mitochondrial enzymes, we quantified this parameter for the tricarboxylic acid -cycle enzyme citrate synthase (CS; Fig. 5D) and the five oxidative phosphorylation (OXPHOS) complexes (Fig. 5E–I; CI–CV). Trolox increased the activity of CS and the OXPHOS enzymes by ~50%, demonstrating that the Trolox-induced increase in activity is not CI specific. Plotting the Trolox-induced increase in V_{max} as a function of the increase in expression of the fully assembled complexes (Fig. 5C) revealed a linear correlation for CI (23), and possibly CV; whereas the activity of CII, CIII, and CIV

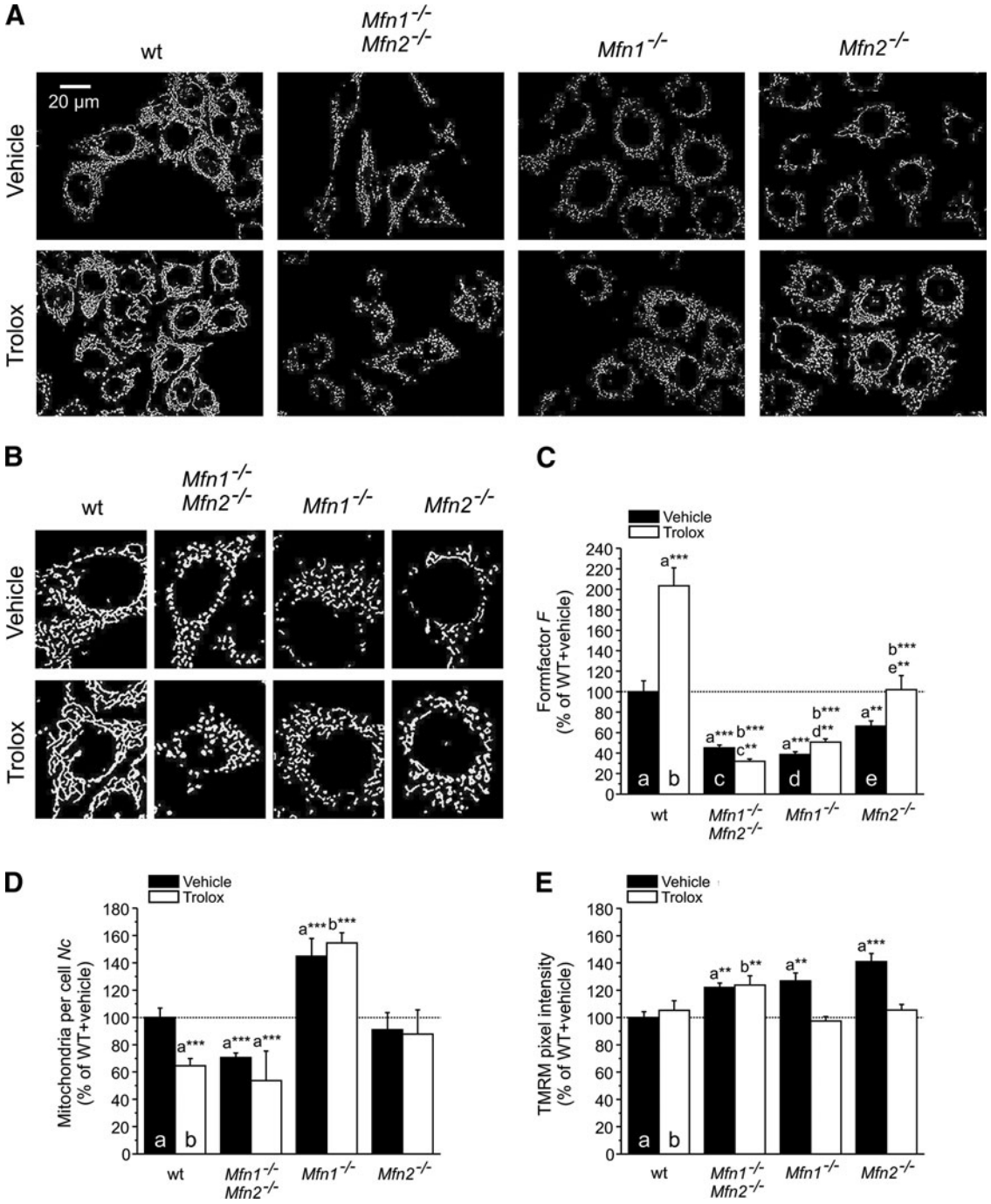

FIG. 4. Effect of Trolox on mitochondrial structure and mitochondrial membrane potential ($\Delta\psi$) in wild-type (wt) and mitofusin knockout cells. (A) Typical examples of background-corrected and binarized microscopy images highlighting mitochondrial structure (*white objects*) in mouse embryonic fibroblasts (MEFs) stained with tetramethyl rhodamine methyl ester (TMRM). Wild-type (wt), mitofusin 1 and 2 double knockout ($Mfn1^{-/-}Mfn2^{-/-}$), mitofusin 1 knockout ($Mfn1^{-/-}$), and mitofusin 2 knockout ($Mfn2^{-/-}$) MEFs are shown. The *upper* and *lower rows* depict vehicle- and Trolox-treated cells, respectively. **(B)** Magnification of single cells in panel **A** for each condition. **(C)** Effect of Trolox treatment on mitochondrial length and degree of branching (reflected by the formfactor *F*). **(D)** Effect of Trolox treatment on the number of mitochondria per cell (*Nc*). **(E)** Effect of Trolox treatment on the average $\Delta\psi$, as reflected by mitochondrial TMRM intensity. In this figure **(C–E)**, significant differences with the indicated condition (a, b, c, d, e) are marked by **($p < 0.01$) and ***($p < 0.001$). The number of cells analyzed in two independent experiments equals: 96 (wt + vehicle), 104 (wt + Trolox), 127 ($Mfn1^{-/-}Mfn2^{-/-}$ + vehicle), 95 ($Mfn1^{-/-}Mfn2^{-/-}$ + Trolox), 103 ($Mfn1^{-/-}$ + vehicle), 87 ($Mfn1^{-/-}$ + Trolox), 112 ($Mfn2^{-/-}$ + vehicle), and 80 ($Mfn2^{-/-}$ + Trolox).

increased supralinear (Fig. 5J). This suggests that Trolox treatment stimulates the activity of CI, and possibly CV, by increasing their protein levels; whereas it stimulates CII, CIII, and CIV activity without affecting these levels.

Trolox does not induce major changes at the transcriptional level

To determine whether the observed Trolox-induced cellular changes were mediated by alterations at the transcriptional level, the latter were quantified in vehicle- and Trolox-treated fibroblasts using microarray analysis (three independent experiments). Statistical analysis revealed no significant changes (Supplementary Fig. S2A). Pathway analysis of the genes with at least a twofold increase (18 genes) or decrease (22 genes) in expression highlighted minor changes in four metabolic pathways (Supplementary Fig. S2B). In agreement with this analysis, Western blotting of the samples used for the microarray revealed lower cellular protein levels of three gene products that were common to these pathways (glycogen synthase 1 [GYS1], aldolase C, fructose-bisphosphate [ALDOC], and enolase 1 [ENO1]; Supplementary Fig. S2C).

Trolox affects cytosolic Ca^{2+} handling

Given the importance of mitochondrial structure and mitofusins in cellular Ca^{2+} signaling (5), we finally determined how Trolox treatment affected hormone-induced cytosolic Ca^{2+} transients. As just demonstrated, Trolox lowers the levels of CM-H_2DCF oxidizing ROS in primary human skin fibroblasts. Previous experiments revealed that H_2O_2 stimulates CM-H_2DCF oxidation in this cell type (12, 21). This suggests that Trolox and H_2O_2 act antagonistically on the levels of CM-H_2DCF oxidizing ROS, thereby affecting Ca^{2+} homeostasis. To investigate the interplay between Trolox, H_2O_2, and cytosolic Ca^{2+} handling, we here cultured fibroblasts in the presence of vehicle (CT) or Trolox and then incubated them for 1 h in the absence or presence of different concentrations of H_2O_2 (Fig. 6A). Subsequently, Ca^{2+} release from the endoplasmic reticulum (ER) was triggered by application of the hormone bradykinin (46) and the kinetics of the cytosolic Ca^{2+} transient were analyzed (Fig. 6B). We avoided applying very high H_2O_2 concentrations (*i.e.*, $>300\ \mu M$), as these induced acute cell shrinkage. To match the maximal H_2O_2 concentration, an equimolar concentration of Trolox ($300\ \mu M$) was used. By itself (Fig. 6B), H_2O_2 did not affect the amplitude (Fig. 6D) but reduced the rate of decay (Fig. 6E) of the cytosolic Ca^{2+} transient. In the absence of H_2O_2, Trolox increased the amplitude and rate of decay (Fig. 6C). These increases were dose dependently antagonized by H_2O_2 (Fig. 6C–E).

Discussion

ROS can function as signaling molecules (sROS) when their levels are below those that trigger oxidative stress (3, 10, 15, 22, 30, 42, 48). Here, we used the antioxidant Trolox to investigate the hypothesis that sROS regulate mitochondrial morphology and function in healthy cells. Our findings support a model in which Trolox-sensitive sROS regulate mitochondrial mitofusin levels and thereby mitochondrial morphology and function (Fig. 7).

Nature of the Trolox-sensitive sROS

Trolox did not affect HEt oxidation but lowered CM-H_2DCF oxidation and cellular lipid peroxidation. This demonstrates that HEt and CM-H_2DCF are oxidized by different types of ROS and suggests that CM-H_2DCF oxidizing sROS induce cellular lipid peroxidation and mediate the downstream effects of Trolox. Acute H_2O_2 application increased the rate of CM-H_2DCF oxidation, whereas both acute and chronic Trolox treatment reduced this rate (9, 12, 21, 23). Similarly, Trolox (this study) and H_2O_2 (11) decreased and increased cellular lipid peroxidation, respectively. These findings suggest that H_2O_2 is responsible for CM-H_2DCF oxidation and lipid peroxidation. However, in a cell-free system, H_2O_2 was unable to stimulate CM-H_2DCF oxidation (16). Instead, the latter was enhanced by the presence of horseradish peroxidase, Fe(II), catalase, copper-zinc superoxide dismutase (CuZnSOD), xanthine oxidase, peroxinitrite ($ONOO^-$), or nitric oxide (*e.g.*, 16, 19). In intact cells, it was demonstrated that the overexpression of the $O_2^{\bullet -}$ detoxifying enzyme CuZnSOD enhanced H_2O_2-induced CM-H_2DCF oxidation (20), suggesting that cells contain catalysts, such as transition metal ions, heme peroxidases, and/or SODs that allow H_2O_2 to indirectly stimulate CM-H_2DCF oxidation. In the light of what has just been stated, it is unlikely that H_2O_2 directly oxidizes CM-H_2DCF inside human skin fibroblasts. Therefore, we conclude that Trolox acts on H_2O_2-derived, CM-H_2DCF oxidizing, ROS. Trolox treatment induced a less oxidized thiol redox environment in the mitochondrial matrix without affecting this parameter in the cytosol. GSH is the most important determinant of the thiol redox environment (36), and H_2O_2 removal is GSH dependent (22). The GSH neo-synthesis inhibitor BSO induced mitochondrial fragmentation and prevented the Trolox-induced increase in mitochondrial filamentation. A previous study revealed that Trolox radicals can act as pro-oxidants when not properly recycled by GSH (34). These data suggest that GSH is necessary for the Trolox-induced effects on mitochondrial morphology.

Trolox stimulates mitofusin-mediated mitochondrial filamentation

A key finding of this study is that Trolox stimulates mitochondrial filamentation and increases the protein levels of mitochondria-attached Mfn2 without altering the levels of Drp1 and Fis1. The fact that identical phenomena were observed in CHO cells demonstrates that this effect is not fibroblast specific. An analysis of mitofusin KO cells demonstrated that Trolox-induced mitochondrial filamentation is mediated by mitofusins. Mechanistically, Trolox-sensitive sROS might not only act directly but could also affect mitofusin stability by the peroxidation of mitochondrial lipids (39). The latter hypothesis is supported by our result that the expression of mitochondrial fission/fusion genes was not affected by Trolox. We further demonstrate that the induction of mitochondrial fragmentation by Drp1 overexpression does not stimulate CM-H_2DCF oxidation, suggesting that increased levels of CM-H_2DCF oxidizing ROS are not a *de facto* consequence of mitochondrial fragmentation. A recent conceptual model by Westermann (47) proposes that mitochondria can exist in

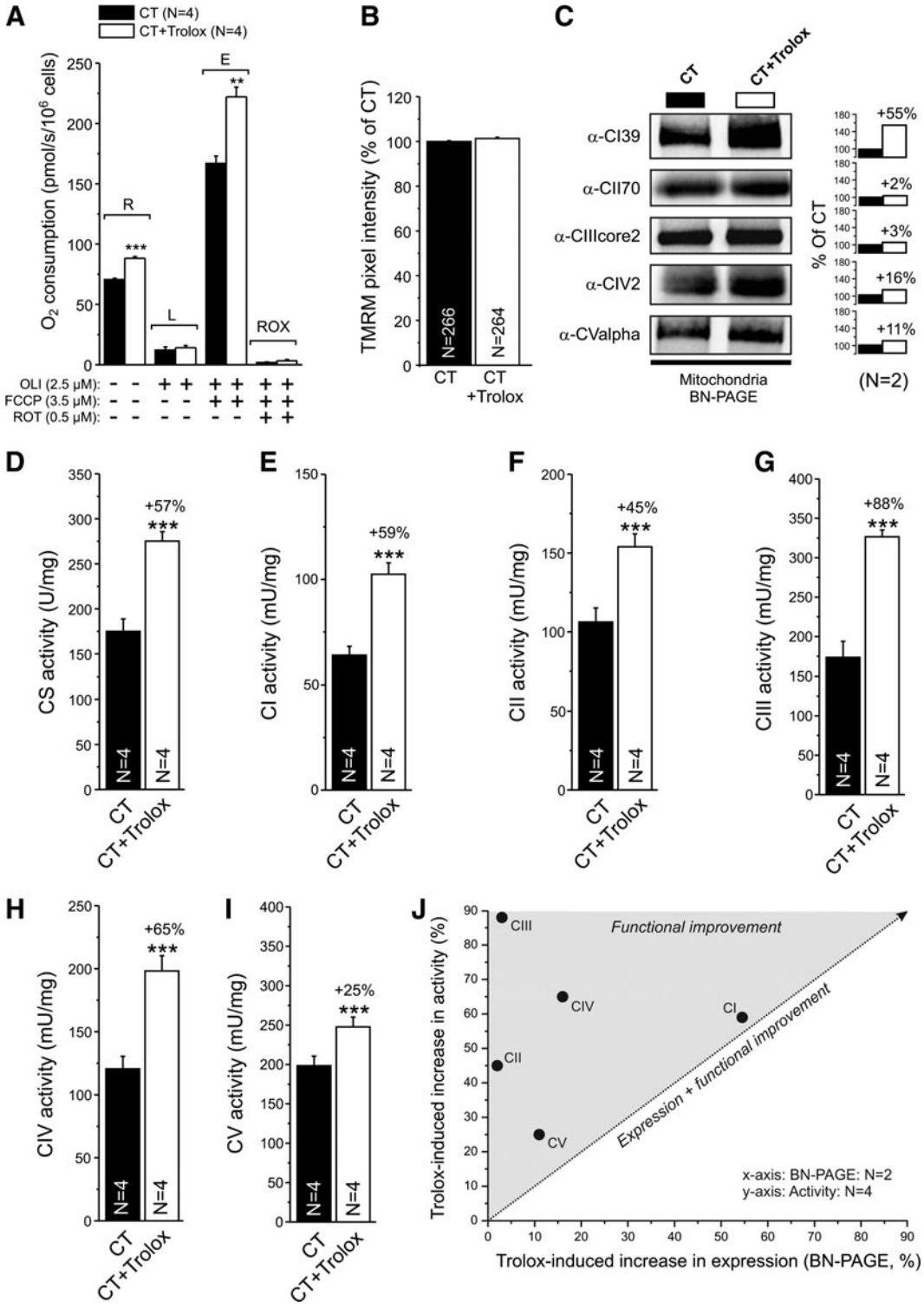

FIG. 5. Effect of Trolox on cellular oxygen consumption, Δψ, expression of fully assembled oxidative phosphorylation (OXPHOS) complexes and maximal activity of citrate synthase (CS), and OXPHOS complexes in human skin fibroblasts. **(A)** Analysis of O_2 consumption in vehicle- (CT) and Trolox-treated cells and the effect of the CV inhibitor oligomycin (OLI), the mitochondrial uncoupler FCCP, and the CI inhibitor rotenone (ROT). Capital letters indicate routine (R), leak (L), maximal (E), and minimal (ROX) O_2 consumption. **(B)** Average $\Delta\psi$, as reflected by mitochondrial TMRM intensity. **(C)** Expression of fully assembled CI to CV, as revealed by blue-native (BN) PAGE electrophoresis of mitoplasts isolated from vehicle (CT)- and Trolox-treated cells (CT + Trolox). The bar graphs indicate the Trolox-induced change in expression. **(D)** Effect of Trolox on CS activity. **(E)** Effect of Trolox on CI activity. **(F)** Effect of Trolox on CII activity. **(G)** Effect of Trolox on CIII activity. **(H)** Effect of Trolox on CIV activity. **(I)** Effect of Trolox on CV activity. **(J)** Relationship between the Trolox-induced increase in expression of the fully assembled complex and maximal activity for CI–CV **(**data taken from panels **C** to **I)**. The dotted line represents a proportional increase in expression and activity. In this figure, significant differences between CT- and the Trolox-treated condition are marked by **($p < 0.01$) and ***($p < 0.001$). Numerals (N) represent the number of individual assays **(A** and **D–I)**, cells **(B)** or independent experiments **(C)**.

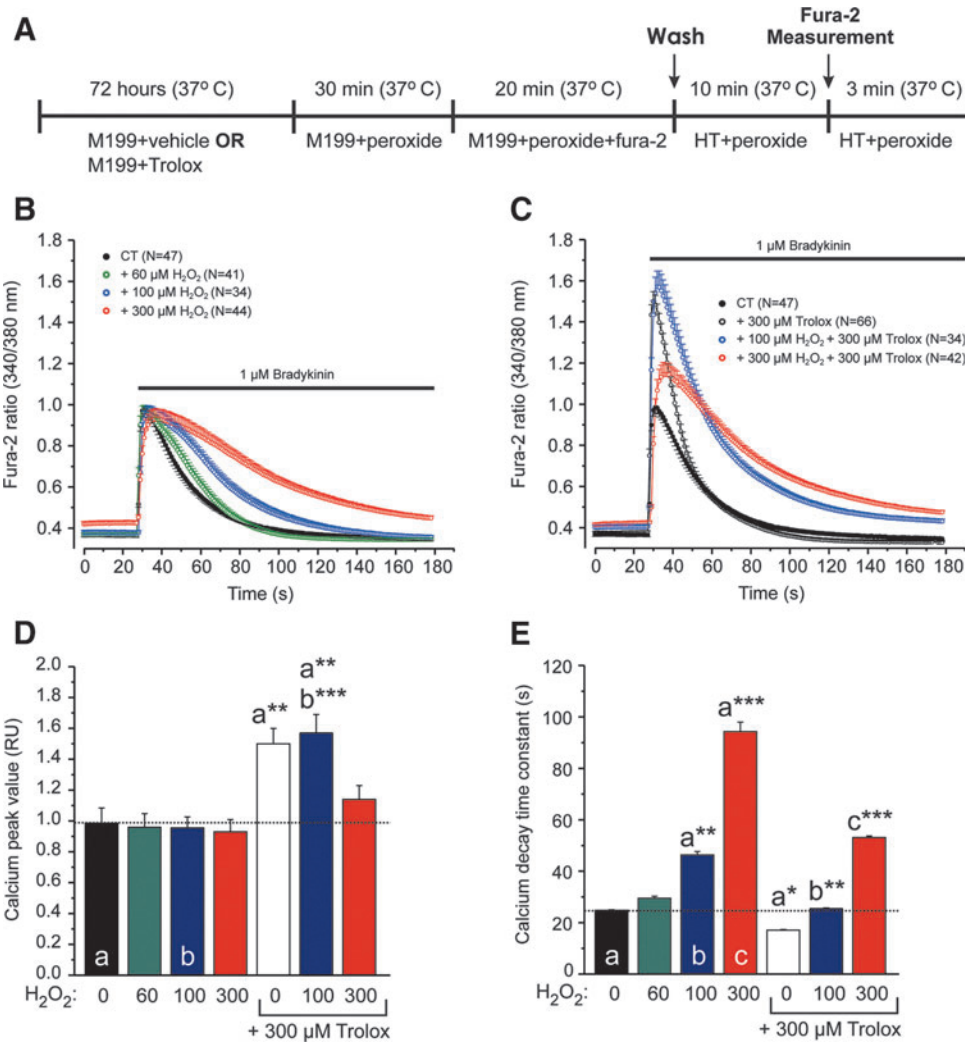

FIG. 6. Effect of Trolox and hydrogen peroxide (H_2O_2) on hormone-induced calcium transients in human skin fibroblasts. (A) Cell incubation protocol for analyzing the effects of Trolox and hydrogen peroxide (H_2O_2) on hormone-stimulated cytosolic Ca^{2+} signals. In this panel, HT indicates HEPES-Tris solution, M199 indicates culture medium, and peroxide indicates H_2O_2. **(B)** Effect of H_2O_2 on bradykinin-induced cytosolic Ca^{2+} transients. **(C)** Effect of Trolox on bradykinin-induced cytosolic Ca^{2+} transients in the absence and presence of H_2O_2. **(D)** Average amplitude of the Ca^{2+} transients for the conditions in panel **B** and **C**. **(E)** Average rate of decay of the Ca^{2+} transients under the conditions in panel **B** and **C**, as determined by fitting a monoexponential function (see Supplementary Materials and Methods). A larger value indicates a slower rate of decay. In panels **D** and **E,** significant differences with the indicated conditions (a, b, c) are marked by *($p<0.05$), **($p<0.01$), or ***($p<0.001$). Numerals (*N*) represent the number of individual cells analyzed in at least three independent experiments. (To see this illustration in color, the reader is referred to the web version of this article at www.liebertpub.com/ars.)

three morphological states: (**I**) a "fragmented state" (low respiratory activity); (**II**) a "normal state" ("normal" respiratory activity); and (**III**) a "hyperfused" state (high respiratory activity). Compatible with this model, our current results suggest that the lowering of Trolox-sensitive CM-H_2DCF-oxidizing sROS stimulates the transition from state **II** to state **III** in healthy human fibroblasts. The Westermann model is also compatible with our results in patient fibroblasts with mitochondrial complex I deficiency (25), where we observed that greatly increased levels of Trolox-sensitive CM-H_2DCF-oxidizing ROS are associated with mitochondrial fragmentation (*i.e.*, the transition from state **II** to state **I**). This suggests that normal levels of Trolox-sensitive CM-H_2DCF-oxidizing sROS are associated with the "normal morphological state," reduced levels of sROS with the "hyperfused morphological state," and increased levels of sROS with the "fragmented state." In this way, cell-controlled changes in sROS levels (for instance, by altering the balance between their production and detoxification) would allow the (co)regulation of mitochondrial morphology, OXPHOS function, and cytosolic calcium handling.

Trolox increases cellular O_2 consumption and mitochondrial enzyme activity

Trolox-treated cells displayed a normal leak O_2 consumption, normal mitochondrial NAD(P)H levels, normal $\Delta\psi$, but an increased routine O_2 consumption. This suggests that in Trolox-treated cells, a new metabolic equilibrium is established in which mitochondrial ATP production is increased. Although microarray analysis revealed no significant changes, combined pathway analysis and Western blot analysis suggests that precursor/energy generation, as well as glucose, hexose, and monosaccharide metabolism are somewhat down-regulated in Trolox-treated cells. The latter is compatible with a slight shift from glycolytic ATP production to mitochondrial (*i.e.*, OXPHOS-mediated) ATP production. The increased routine and maximal O_2 consumption in Trolox-treated cells can be explained by the fact that both CS and the OXPHOS complexes displayed an increased maximal activity. Alternatively, evidence has been provided that Mfn2 is directly involved in substrate oxidation and the expression regulation of OXPHOS proteins (52). Trolox increased the

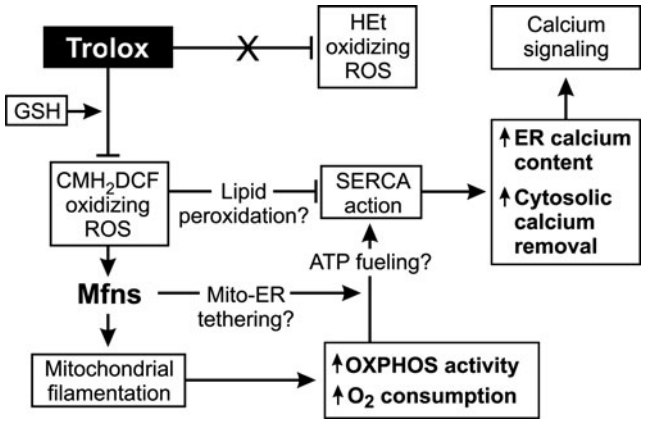

FIG. 7. Regulation of mitochondrial morphology and OXPHOS by Trolox-sensitive endogenous signaling reactive oxygen species (sROS). Trolox reduces the levels of endogenous CM-H_2DCF oxidizing signaling ROS (sROS) but not HEt oxidizing sROS in a glutathione (GSH)-dependent manner. This leads to increased levels of mitochondria-attached mitofusins and ensuing mitochondrial filamentation. The latter is associated with increased OXPHOS activity, O_2 consumption, and sarcoplasmatic-endoplasmatic reticulum Ca^{2+} ATPase (SERCA) action, thereby affecting cellular calcium handling (see Discussion for details).

expression of fully assembled CI, CIV, and CV; whereas the expression of CII and CIII was not affected. Moreover, microarray analysis revealed that the expression of CS and OXPHOS genes was not stimulated by Trolox. These results suggest that mitochondrial membrane-embedded or -attached proteins are directly affected by Trolox with regard to their maximal catalytic activity (CS, CI, CII, CIII, CIV, and CV) and/or stability (CI, CIV, and CV). Mechanistically, the direct Trolox effect might be related to the observation that Trolox can repair proteins which have been oxidized by ROS (4). In addition, Trolox prevented the degradation of cardiolipin (41), a mitochondria-specific lipid involved in OXPHOS complex/super-complex formation (17).

Trolox alters cytosolic Ca^{2+} handling in hormone-stimulated cells

Trolox increased the amplitude and rate of decay of bradykinin-induced cytosolic Ca^{2+} transients. Using primary human skin fibroblasts, we have established (45, 46) that this amplitude is a measure of ER Ca^{2+} content (ERCa), whereas the rate of decay reflects ATP-dependent Ca^{2+} uptake into the ER by the sarcoplasmatic-endoplasmatic reticulum Ca^{2+} ATPase (SERCA). In this sense, our current results agree with our previous finding that Trolox increases ERCa (7). We previously observed that the Ca^{2+}-stimulated maximal mitochondrial ATP production was not affected in Trolox-treated primary human skin fibroblasts (7), suggesting that SERCA fueling with mitochondria-derived ATP is not increased by Trolox. However, mitofusins are important in the physical tethering and functional coupling of mitochondria and the ER (5). So, increased mitofusin expression might reduce the distance between the ER and mitochondria, allowing a more efficient local ATP delivery from mitochondria to SERCA pumps in Trolox-treated cells. The latter could explain the higher rate of SERCA-mediated Ca^{2+} decay in Trolox-treated cells. Trolox and H_2O_2 displayed opposite effects on CM-H_2DCF-oxidation, and Trolox-induced changes in Ca^{2+} dynamics were dose-dependently antagonized by H_2O_2. This suggests that Trolox-sensitive, CM-H_2DCF oxidizing, ROS play a role in controlling ERCa. The latter hypothesis is compatible with our previous analysis of primary fibroblasts from patients with isolated CI deficiency, which revealed a negative correlation between the levels of H_2DCF-oxidizing ROS and ERCa (7). It is also supported by experiments which demonstrate that H_2O_2 dose-dependently reduces ER Ca^{2+} uptake through SERCA inhibition, possibly due to the enhanced peroxidation of the ER membrane (14). The latter is compatible with our current observation that Trolox reduces oxidation of the lipid peroxidation sensor C11, which also resides in ER membranes (11). Alternatively, CM-H_2DCF-oxidizing ROS might prevent the influx of Ca^{2+} across the plasmamembrane during Bk-induced Ca^{2+} release from the ER (capacitative Ca^{2+} entry [CCE]). This would mean that Trolox treatment increases CCE during hormone stimulation, thereby increasing the amplitude of the cytosolic Ca^{2+} transient. However, the presence or absence of extracellular Ca^{2+} did not affect the kinetics of Bk-induced Ca^{2+} signals (46), and basal levels of endogenous ROS and Trolox did not affect Ca^{2+} entry across the plasma membrane on hormone-induced ER Ca^{2+} release in vascular endothelial cells (9). This argues against the modulation of CCE by CM-H_2DCF-oxidizing sROS.

Materials and Methods

Cell culture and enzyme activity measurements

Control (CT) human skin fibroblasts (#5120) were obtained from a healthy individual. Biopsies were performed following informed consent and according to the relevant Institutional Review Boards. Fibroblasts were cultured as previously described (6). CHO cells, HeLa cells, and immortalized MEFs were cultured as described in the Supplementary Materials and Methods. Trolox was dissolved in ethanol and added to the culture medium. Unless otherwise stated, the cells were cultured in the presence of vehicle- or Trolox (0.5 m*M*, 96 h) in a humidified atmosphere (95% air, 5% CO_2) at 37°C. The activity of mitochondrial enzymes was determined as previously described (35).

Determination of ROS levels, lipid peroxidation, $\Delta\psi$, NAD(P)H levels, thiol redox state, and Ca^{2+} dynamics

Levels of cellular ROS were determined by quantifying the oxidation rate of CM-H_2DCF (Invitrogen) and HEt as previously described (11, 24, 43, 44). An analysis of cellular lipid peroxidation was performed by measuring the green (oxidized) to red (reduced) fluorescence ratio of C11-BODIPY$^{581/591}$ (C11; Invitrogen) as previously described (11, 24, 43). Mitochondrial tetramethyl rhodamine methyl ester (TMRM; Invitrogen) staining was used to estimate $\Delta\psi$; staining with TMRM or rhodamine 123 (Invitrogen) was used to quantify mitochondrial morphology. The TMRM and R123 approaches were previously described in detail (6, 24, 26). Measurements of mitochondrial NAD(P)H autofluorescence were carried out as described earlier (43). Mitochondrial and cytosolic redox state was quantified using a redox-sensitive GFP (roFGP1) as previously described (43). Cytosolic-free Ca^{2+} levels were quantified as described in the Supplementary Materials and Methods.

High-resolution respirometry

Cellular O_2 consumption was measured as described in the Supplementary Materials and Methods.

Western blotting of mitochondria-enriched fractions and whole cell homogenates

Mitochondria-enriched fractions were prepared (see Supplementary Materials and Methods), and exactly 20 μg of protein was loaded on a sodium dodecyl sulfate–polyacrylamide gel electrophoresis (PAGE) gel for each condition. Proteins were transferred onto PVDF membranes (Millipore) using a Biorad blotting system. Blots were incubated with monoclonal primary antibodies against Mfn2 (Sigma), dynamin-related protein 1 (Dlp1/Drp1; BD Biosciences), hFis1 (Imgenics), and mitochondrial porin (Calbiochem). A fluorescent secondary antibody was used, which was detected using an Odyssey Imaging system (Li-Cor). Western blotting of whole cell homogenates was performed as described in the Supplementary Materials and Methods.

Blue-native PAGE electrophoresis of OXPHOS complexes in mitochondria-enriched fractions

Blue-native PAGE analysis of mitoplasts was performed as previously described (23, 44).

Gene expression profiling and pathway analysis

Independent cell cultures of vehicle- ($N=3$) and Trolox-treated ($N=3$) fibroblasts were used to isolate mRNA, and gene expression was analyzed using an Affymetrix GeneChip Human Exon 1.0 ST array containing all known human genes (Affymetrix, Inc.), according to the manufacturer's instructions (see Supplementary Materials and Methods).

Image processing and data analysis

Image processing was performed using Image Pro Plus 6.3 software (Media Cybernetics). Data analysis was carried out using Origin Pro 6.1 (OriginLab Corp.). Averages are presented as the mean ± standard error of the mean, unless stated otherwise. Statistical differences were determined using either a two-population or a one-population Student's *t*-test (Bonferroni corrected).

Acknowledgments

This research was supported by grants of ZON (Netherlands Organization for Health Research and Development: #903-46-176), NWO (Netherlands Organization for Scientific Research: #911-02-008), the Dutch Ministry of Economic Affairs ("Innovatieve Onderzoeks Projecten" [IOP]: #IGE05003), the CSBR (Centers for Systems Biology Research) initiative from NWO (No: CSBR09/013V), the Heinrich Heine University (Düsseldorf, Germany), and the Energy4All foundation. The authors are grateful to Dr. D.C. Chan (California Institute of Technology, Pasadena, CA) for generating and Dr. L. Scorrano (Dulbecco-Telethon Institute, Venetian Institute of Molecular Medicine, Padova, Italy) for providing the wild-type, *Mfn1*$^{-/-}$, *Mfn2*$^{-/-}$ and *Mfn1*$^{-/-}$*Mfn2*$^{-/-}$ MEF cell lines; Dr. S. J. Remington (University of Oregon, Eugene, OR) for supplying the cDNA's encoding roGFP1; and Dr. R. J. Youle (NIH, Bethesda, MD) for providing the inducible Drp1-expressing HeLa cell line. MitoQ was kindly donated by Dr. M. Murphy (MRC, Mitochondrial Biology Unit, Cambridge, United Kingdom). The authors thank the following members of the Dept. of Biochemistry NCMLS for performing Western blotting (Mr. Varun K. Praphakar), fura-2 measurements (Dr. H.J. Visch), ATeam analysis (Dr. J.J. Esseling and Mr. A. Klymov), and experiments with the inducible Drp1-expressing HeLa cell line (Mr. D. Lam). They also acknowledge Dr. Marcel Nelen (Department of Human Genetics, RUNMC) for assistance with gene expression analysis.

Author Disclosure Statement

No competing financial interests exist.

References

1. Benard G and Rossignol R. Ultrastructure of the mitochondrion and its bearing on functions and bioenergetics. *Antioxid Redox Signal* 10: 1313–1342, 2008.
2. Brown GC and Borutaite V. There is no evidence that mitochondria are the main source of reactive oxygen species in mammalian cells. *Mitochondrion* 12: 1–4, 2011.
3. D'Autréaux B and Toledano MB. ROS as signalling molecules: mechanisms that generate specificity in ROS homeostasis. *Nat Rev Mol Cell Biol* 8: 813–824, 2007.
4. Davies MJ, Forni LG, and Willson RL. Vitamin E analogue Trolox C. E.s.r. and pulse-radiolysis studies of free-radical reactions. *Biochem J* 255: 513–522, 1988.
5. De Brito OM and Scorrano L. Mitofusin 2 tethers endoplasmic reticulum to mitochondria. *Nature* 456: 605–610, 2008.
6. Distelmaier F, Koopman WJ, Testa ER, de Jong AS, Swarts HG, Mayatepek E, Smeitink JA, and Willems PH. Life cell quantification of mitochondrial membrane potential at the single organelle level. *Cytometry A* 73A: 129–138, 2008.
7. Distelmaier F, Visch HJ, Smeitink JA, Mayatepek E, Koopman WJ, and Willems PH. The antioxidant Trolox restores mitochondrial membrane potential and Ca^{2+}-stimulated ATP production in human complex I deficiency. *J Mol Med* 87: 515–522, 2009.
8. Fan X, Hussien R, and Brooks GA. H_2O_2-induced mitochondrial fragmentation in C2C12 myocytes. *Free Radic Biol Med* 49: 1646–1654, 2010.
9. Florea SM and Blatter LA. The effect of oxidative stress on Ca^{2+} release and capacitative Ca^{2+} entry in vascular endothelial cells. *Cell Calcium* 43: 405–415, 2008.
10. Finkel T. Signal transduction by reactive oxygen species. *J Cell Biol* 194: 7–15, 2011.
11. Forkink M, Smeitink JA, Brock R, Willems PH, and Koopman WJ. Detection and manipulation of mitochondrial reactive oxygen species in mammalian cells. *Biochim. Biophys Acta Bioenergetics* 1797: 1034–1044, 2010.
12. Gibson GE and Huang HM. Mitochondrial enzymes and endoplasmic reticulum calcium stores as targets of oxidative stress in neurodegenerative diseases. *J Bioenerg Biomembr* 36: 335–340, 2004.
13. Gomes LC, Di Benedetto G, and Scorrano L. During autophagy mitochondria elongate, are spared from degradation and sustain cell viability. *Nature Cell Biol* 13: 589–598, 2011.
14. Grover AK, Samson SE, and Misquitta CM. Sarco(endo)plasmic reticulum Ca^{2+} pump isoform SERCA3 is more resistant than SERCA2b to peroxide. *Am J Physiol.* 273: 420–425, 1997.

15. Gülden M, Jess A, Kammann J, Maser E, and Seibert H. Cytotoxic potency of H_2O_2 in cell cultures: impact of cell concentration and exposure time. *Free Rad Biol Med* 49: 1298–1305, 2010.
16. Hempel SL, Buettner GR, O'Malley YQ, Wessels DA, and Flaherty DM. Dihydrofluorescein diacetate is superior for detecting intracellular oxidants: comparison with 2′,7′-dichlorodihydrofluorescein diacetate, 5(and 6)-carboxy-2′,7′-dichlorodihydrofluorescein diacetate, and dihydrorhodamine 123. *Free Radic Biol Med* 27: 146–159, 1999.
17. Houtkooper RH and Vaz FM. Cardiolipin, the heart of mitochondrial metabolism. *Cell Mol Life Sci* 65: 2493–2506, 2008.
18. Jendrach M, Mai S, Pohl S, Vöth M, and Bereiter-Hahn J. Short- and long-term alterations of mitochondrial morphology, dynamics and mtDNA after transient oxidative stress. *Mitochondrion* 8: 293–304, 2008.
19. Keller A, Mohamed A, Dröse S, Brandt U, Fleming I, and Brandes RP. Analysis of dichlorodihydrofluorescein and dihydrocalcein as probes for the detection of intracellular reactive oxygen species. *Free Radic Res* 38: 1257–1267, 2004.
20. Kim YM, Lim JM, Kim BC, and Han S. Cu,Zn-superoxide dismutase is an intracellular catalyst for the H_2O_2-dependent oxidation of dichlorodihydrofluorescein. *Mol Cells* 21: 161–165, 2006.
21. Koopman WJH, Grefte S, Smeitink JA, and Willems PH. Simultaneous quantification of oxidative stress and cell spreading using 5-(and-6)-chloromethyl-2′,7′-dichlorofluorescein. *Cytometry A* 69A: 1184–1192, 2006.
22. Koopman WJH, Nijtmans LG, Dieteren CE, Roestenberg P, Valsecchi F, Smeitink JA, and Willems PH. Mammalian mitochondrial complex I: biogenesis, regulation and reactive oxygen species generation. *Antioxid Redox Signal* 12: 1431–1470, 2010.
23. Koopman WJH, Verkaart S, van Emst-de Vries SE, Grefte S, Smeitink JA, Nijtmans LG, and Willems PH. Mitigation of NADH: ubiquinone oxidoreductase deficiency by chronic Trolox treatment. *Biochim Biophys Acta* 1777: 853–859, 2008.
24. Koopman WJH, Verkaart S, Visch HJ, van der Westhuizen FH, Murphy MP, van den Heuvel LW, Smeitink JA, and Willems PH. Inhibition of complex I of the electron transport chain causes oxygen radical-mediated mitochondrial outgrowth. *Am J Physiol Cell Physiol* 288: C1440–C1450, 2005.
25. Koopman WJH, Verkaart S, Visch HJ, van Emst-de Vries SE, Nijtmans LG, Smeitink JA, and Willems PH. Human NADH:ubiquinone oxidoreductase deficiency: radical changes in mitochondrial morphology? *Am J Physiol Cell Physiol* 293: C22–C29, 2007.
26. Koopman WJH, Visch HJ, Smeitink JA, and Willems PH. Simultaneous quantitative measurement and automated analysis of mitochondrial morphology, mass, potential, and motility in living human skin fibroblasts. *Cytometry A* 69A: 1–12, 2006.
27. Koopman WJH, Willems PHGM, and Smeitink JAM. Monogenic mitochondrial disorders. *N Engl J Med* 366: 1132–1141, 2012.
28. Mahon KP, Potocky TB, Blair D, Roy MD, Stewart KM, Chiles TC, and Kelley SO. Deconvolution of the cellular oxidative stress response with organelle-specific peptide conjugates. *Chem Biol* 14: 923–930, 2007.
29. Mai S, Klinkenberg M, Auburger G, Bereiter-Hahn J, and Jendrach M. Decreased expression of Drp1 and Fis1 mediates mitochondrial elongation in senescent cells and enhances resistance to oxidative stress through PINK1. *J Cell Sci* 123: 917–926, 2010.
30. Murphy MP, Holmgren A, Larsson NG, Halliwell B, Chang CJ, Kalyanaraman B, Rhee SG, Thornalley PJ, Partridge L, Gems D, Nyström T, Belousov V, Schumacker PT, and Winterbourn CC. Unraveling the biological roles of reactive oxygen species. *Cell Metab* 13: 361–366, 2011.
31. Parone PA, Da Cruz S, Tondera D, Mattenberger Y, James DI, Maechler P, Barja F, and Martinou JC. Preventing mitochondrial fission impairs mitochondrial function and leads to loss of mitochondrial DNA. *PLoS One* 3: e3257, 2008.
32. Qi X, Disatnik MH, Shen N, Sobel RA, and Mochly-Rosen D. Aberrant mitochondrial fission in neurons induced by delta protein kinase C under oxidative stress conditions, *in vivo*. *Mol Biol Cell* 22: 256–265, 2010.
33. Rakovic A, Grünewald A, Kottwitz J, Brüggemann N, Pramstaller P, Lohmann K, and Klein C. Mutations in PINK1 and Parkin impair ubiquitination of mitofusins in human fibroblasts. *PLoS One* 6: e16746, 2011.
34. Raspor P, Plesnicar S, Gazdag Z, Pesti M, Miklavcic M, Lah B, Logar-Marinsek R, and Poljsak B. Prevention of intracellular oxidation in yeast: the role of vitamin E analogue, Trolox (6-hydroxy-2,5,7,8-tetramethylkroman-2-carboxyl acid). *Cell Biol Int* 29: 57–63, 2005.
35. Rodenburg RJ. Biochemical diagnosis of mitochondrial disorders. *J. Inherit Metab Dis* 34: 283–92, 2011.
36. Schafer FQ and Buettner GR. Redox environment of the cell as viewed through the redox state of the glutathione disulfide/glutathione couple. *Free Radic Biol Med* 30: 1191–1212, 2001.
37. Storz P. Forkhead homeobox type O transcription factors in the responses to oxidative stress. *Antioxid Redox Signal* 14: 593–605, 2011.
38. Tafazoli S, Wright JS, and O'Brien PJ. Prooxidant and antioxidant activity of vitamin E analogues and troglitazone. *Chem Res Toxicol* 18: 1567–1574, 2005.
39. Tanaka A, Cleland MM, Xu S, Narendra DP, Suen DF, Karbowski M, and Youle RJ. Proteasome and p97 mediate mitophagy and degradation of mitofusins induced by Parkin. *J Cell Biol* 191: 1367–1380, 2010.
40. Twig G and Shirihai OS. The interplay between mitochondrial dynamics and mitophagy. *Antioxid Redox Signal* 14: 1939–1951, 2011.
41. Umansky V, Ratter F, Lampel S, Bucur M, Schirrmacher V, and Ushmorov A. Inhibition of nitric-oxide-mediated apoptosis in Jurkat leukemia cells despite cytochrome *c* release. *Exp Cell Res* 265: 274–282, 2001.
42. Valko M, Leibfritz D, Moncol J, Cronin MT, Mazur M, and Telser J. Free radicals and antioxidants in normal physiological functions and human disease. *Int J Biochem Cell Biol* 39: 44–84, 2007.
43. Verkaart S, Koopman WJ, Cheek J, van Emst-de Vries SE, van den Heuvel LW, Smeitink JA, and Willems PH. Mitochondrial and cytosolic thiol redox state are not detectably altered in isolated human NADH:ubiquinone oxidoreductase deficiency. *Biochim Biophys Acta* 1772: 1041–1051, 2007.
44. Verkaart S, Koopman WJ, Nijtmans LG, van den Heuvel LW, Smeitink JA, and Willems PH Superoxide activity is inversely related to complex I activity in inherited complex I deficiency. *Biochim Biophys Acta* 1772: 373–381, 2007.
45. Visch HJ, Koopman WJ, Leusink A, van Emst-de Vries SE, van den Heuvel LW, Willems PH, and Smeitink JA. Decreased agonist-stimulated mitochondrial ATP production caused by a pathological reduction in endoplasmic reticulum calcium content in human complex I deficiency. *Biochim Biophys Acta* 1762: 115–123, 2006.
46. Visch HJ, Rutter GA, Koopman WJ, Koenderink JB, Verkaart S, de Groot T, Varadi A, Mitchell KJ, van den Heuvel LP, Smeitink JAM, and Willems PHGM. Inhibition of mitochondrial Na^+-Ca^{2+} exchange restores agonist-induced ATP

production and Ca^{2+} handling in human complex I deficiency. *J Biol Chem* 279: 40328–40336, 2004.
47. Westermann B. Bioenergetic role of mitochondrial fusion and fission. *Biochim Biophys Acta* PMID: 22409868, 2012; [Epub ahead of print]; DOI: 10.1016/j.bbabio.2012.02.033.
48. Winterbourn CC. Reconciling the chemistry and biology of reactive oxygen species. Nat Chem Biol 4: 278–286, 2008.
49. Wu S, Zhou F, and Zhang Z. Mitochondrial oxidative stress causes mitochondrial fragmentation via differential modulation of mitochondrial fission-fusion proteins. *FEBS J* 278: 941–954, 2011.
50. Yu T, Jhun BS, and Yoon Y. High-glucose stimulation increases reactive oxygen species production through the calcium and mitogen-activated protein kinase-mediated activation of mitochondrial fission. *Antioxid Redox Signal* 14: 524–437, 2011.
51. Yu T, Robotham JL, and Yoon Y. Increased production of reactive oxygen species in hyperglycemic conditions requires dynamic change of mitochondrial morphology. *Proc Natl Acad Sci U S A* 103: 2653–2658, 2006.
52. Zorzano A, Liesa M, Sebastian D, Segales J, and Palacin M. Mitochondrial fusion proteins: dual regulators of morphology and metabolism. *Semin Cell Dev Biol* 21: 566–574, 2010.

Address correspondence to:
Dr. Werner J.H. Koopman
286 Biochemistry
Nijmegen Centre for Molecular Life Sciences
Radboud University Nijmegen Medical Centre
P.O. Box 9101
NL-6500 HB Nijmegen
The Netherlands

E-mail: w.koopman@ncmls.ru.nl

Date of first submission to ARS Central, October 11, 2011; date of final revised submission, May 5, 2012; date of acceptance, May 5, 2012.

Abbreviations Used

$\Delta\psi$ = mitochondrial membrane potential
ALDOC = aldolase C, fructose-bisphosphate
BN = blue-native
BSO = L-buthionine-(S,R)-sulphoximine
CCE = capacitative Ca^{2+} entry
CHO = Chinese Hamster Ovary
CM-H_2DCF = 5-(and-6)-chloromethyl-2′,7′-dichlorodihydro-fluorescein
CS = citrate synthase
CuZnSOD = copper-zinc superoxide dismutase
Drp1 = dynamin-related protein 1
ENO2 = enolase 2
ER = endoplasmic reticulum
ERCa = ER Ca^{2+} content
ETC = electron transport chain
F = mitochondrial formfactor
GSH = glutathione
GYS1 = glycogen synthase 1
HEt = hydroethidium
hFis1 = human fission protein 1
H_2O_2 = hydrogen peroxide
MEF = mouse embryonic fibroblasts
Mfn1 = mitofusin 1
Mfn1$^{-/-}$ = mitofusin 1 knockout
Mfn2 = mitofusin 2
Mfn2$^{-/-}$ = mitofusin 2 knockout
Mfn1$^{-/-}$*Mfn2*$^{-/-}$ = mitofusin 1 and 2 double knockout
MIM = mitochondrial inner membrane
MitoQ = mitoquinone
Nc = number of mitochondria per cell
OXPHOS = oxidative phosphorylation
PAGE = polyacrylamide gel electrophoresis
PMF = proton motive force
SERCA = sarcoplasmatic-endoplasmatic reticulum Ca^{2+} ATPase
sROS = signaling reactive oxygen species
TMRM = tetramethyl rhodamine methyl ester